ELSEVIER

Journal of Quantitative Spectroscopy & Radiative Transfer 87 (2004) 243–259

Journal of Quantitative Spectroscopy & Radiative Transfer

www.elsevier.com/locate/jqsrt

A successive order of scattering model for solving vector radiative transfer in the atmosphere

Qilong Min*, Minzheng Duan

Atmospheric Sciences Research Center, State University of New York, Albany NY 12203, USA

Received 23 April 2003; accepted 17 December 2003

Abstract

A full vector radiative transfer model for vertically inhomogeneous plane–parallel media has been developed by using the successive order of scattering approach. In this model, a fast analytical expansion of Fourier decomposition is implemented and an exponent-linear assumption is used for vertical integration. An analytic angular interpolation method of post-processing source function is also implemented to accurately interpolate the Stokes vector at arbitrary angles for a given solution. It has been tested against the benchmarks for the case of randomly orientated oblate spheroids, illustrating a good agreement for each stokes vector (within 0.01%). Sensitivity tests have been conducted to illustrate the accuracy of vertical integration and angle interpolation approaches. The contribution of each scattering order for different optical depths and single scattering albedos are also analyzed.

Keywords: Polarization; Successive order of scattering; Radiative transfer

1. Introduction

Polarimetric measurements of atmospheric radiation have been demonstrated significant advantages in retrieving atmospheric aerosol properties, determining size and shape of scattering particles, and discriminating surface and atmospheric contributions [1–4]. These essential advantages are due to polarization characteristics exhibited by radiation scattering by molecules and aerosol and cloud particles, and also due to experimental merits for a relative measurement of polarization that could achieve high accuracy (0.1% for the linear polarization). Observations of polarization of reflected or transmitted light from an atmosphere will provide additional constrains for interpreting photometric measurements, and improve knowledge of the atmospheric constituents. Numerous instruments with

* Corresponding author. Tel.: +1-518-437-8741; fax: +1-518-437-8758.
E-mail address: min@asrc.cestm.albany.edu (Q. Min).

0022-4073/$ - see front matter © 2003 Elsevier Ltd. All rights reserved.
doi:10.1016/j.jqsrt.2003.12.019

polarization capability have been deployed on various platforms [5–11]. To fully exploit the potentials of polarimetric measurements requires an accurate and fast vector radiative transfer model to interpret observations and to retrieve atmospheric properties [12–14].

Several vector radiative transfer codes have been developed based on the adding–doubling method [15,16]. Recently, an extension of the scalar discrete ordinate theory to solve the 4-vector problem for the complete set of Stokes parameters has been reported [17,18]. However, these vector radiative transfer codes do not separate the contribution of each scattering order, which will provide insights of radiation absorption process when scattering evens take place. By computing the contribution of each scattering order, the successive order of scattering (SOS) method is physically straightforward and is easier to analyze the importance and characteristics of scattering–absorption processes. Since the SOS method traces the photons for each scattering event, the inhomogeneous structure of the medium as well as gaseous absorption process can be incorporated in the calculation in terms of integration along the photon path [19]. Further, the SOS method is very helpful for parameterization of radiative transfer for fast computation in remote sensing and global climate modeling. It is also well known that the disadvantage of the SOS method is the substantial computation needed to converge the intensity solution, particularly for an optically thick medium. However, we mostly deal with polarization for aerosols and cirrus clouds that are normally optical thin. For applications to simulate high resolution spectra of absorption bands, in particular, the single scattering albedo is low for absorption lines and the SOS method needs only a few scattering orders to reach convergence. Therefore, for simulating the polarization of radiative transfer in the atmosphere, the SOS method may have substantial advantages over other methods. In this paper we develop a full vector radiative transfer code for plane–parallel media using the successive order scattering method coupled with discretization and interpolation principles. The detail description of the algorithm is given in Section 2. We modify the Fourier decomposition of scattering matrix developed by Siewert [20] to be easily imbedded into a radiative transfer code. In Section 3, various tests and comparisons with the benchmark are discussed.

2. Vector radiative transfer equation

Radiation can be fully described by Stokes parameters, $\vec{\mathbf{I}} = [I, Q, U, V]^{\mathrm{T}}$. Its propagation and re-distribution in plain parallel scattering and absorbing medium can be expressed as [21]

$$\mu \frac{\mathrm{d}\vec{\mathbf{I}}(\tau,\mu,\phi)}{\mathrm{d}\tau} = -\vec{\mathbf{I}}(\tau,\mu,\phi) + \frac{\omega}{4\pi}\int_0^{2\pi}\int_{-1}^{1} \vec{\mathbf{M}}(\tau,\mu,\varphi;\mu',\phi')\vec{\mathbf{I}}(\tau,\mu',\phi')\,\mathrm{d}\mu'\,\mathrm{d}\phi' + \frac{\omega}{4\pi} F_0 \exp(-\tau/\mu_0)\vec{\mathbf{M}}(\tau,\mu,\phi;-\mu_0,\phi_0)[1,0,0,0]^{\mathrm{T}} + (1-\omega)B(T)[1,0,0,0]^{\mathrm{T}}, \quad (1)$$

where $\boldsymbol{\mu}$ is the cosine of the polar angle, positive for downward and minus for upward, $\boldsymbol{\phi}$ is the azimuth angle relative to the solar beam, $\boldsymbol{\tau}$ is the optical depth, $\boldsymbol{\omega}$ is the single-scattering albedo, $\boldsymbol{F}_0$ is the extraterrestrial solar incident flux, μ_0 and ϕ_0 are the cosine of the solar zenith and the solar azimuth angle, respectively, $\boldsymbol{B}$ is the Planck function and $\vec{\mathbf{M}}$ is the phase matrix (Mueller matrix) of scattering of 4×4 order. Superscript T represents the transpose of matrix. In Eq. (1), the

second term is the contribution of multiple scattering, the third term is single scattering contribution from light incident on the upper boundary, and the fourth is contribution of the thermal emission. Based on the optical properties of media, one or more terms often can be ignored. In the visible and near-infrared wavelength region, the fourth term is ignored. Further, the Mueller matrix $\vec{\mathbf{M}}$ is obtained by rotational transform of the single-scattering phase matrix $\vec{\mathbf{P}}$

$$\vec{\mathbf{P}} = \begin{bmatrix} a_1 & b_1 & 0 & 0 \\ b_1 & a_2 & 0 & 0 \\ 0 & 0 & a_3 & b_2 \\ 0 & 0 & -b_2 & a_4 \end{bmatrix}. \tag{2}$$

As discussed by van de Hulst [22], the phase matrix, which contains six real functions, has more general applications including scattering by nonspherical particles [18].

For the radiative transfer in atmospheric application, the Stokes components I and Q of scattered field are symmetric in $\phi - \phi'$, U and V are anti-symmetric in $\phi - \phi'$, therefore, the Stokes vector $\vec{\mathbf{I}}$ and Muller matrix $\vec{\mathbf{M}}$ can be decomposed as follow:

$$\vec{\mathbf{I}} = \begin{bmatrix} I \\ Q \\ U \\ V \end{bmatrix} = \sum_{m=0}^{2M} \begin{bmatrix} I_m \cos m(\phi - \phi_0) \\ Q_m \cos m(\phi - \phi_0) \\ U_m \sin m(\phi - \phi_0) \\ V_m \sin m(\phi - \phi_0) \end{bmatrix}, \tag{3}$$

$$\vec{\mathbf{M}} = \frac{1}{2}\vec{\mathbf{M}}_0^{\mathrm{c}} + \sum_{m=1}^{2M-1} [\vec{\mathbf{M}}_m^{\mathrm{c}} \cos m(\phi - \phi') + \vec{\mathbf{M}}_m^{\mathrm{s}} \sin m(\phi - \phi')], \tag{4}$$

where $\vec{\mathbf{M}}^{\mathrm{c}}$ and $\vec{\mathbf{M}}^{\mathrm{s}}$ stand for cosine mode and sine mode, respectively. For each Fourier component, we have the radiative transfer equation in the same form as Eq. (1).

2.1. Algorithm for vector successive order of scattering (VSOS)

The SOS method is an integral solution approach to solve radiative transfer problems. It can be directly applied to absorption medium to understand the absorption processes in terms of integration along the line path when scattering events take place. To speed up the calculation, we compute the successive scattering of each order based on discrete ordinate and interpolating over optical depth. For the scattered radiation field, the summation of contributions of all scattering orders in each Fourier component can be described as

$$\vec{\mathbf{I}}(\tau, \mu) = \sum_{n=1}^{N} \vec{\mathbf{I}}_n(\tau, \mu), \tag{5}$$

where the subscription n stands for the scattering order, and the index N represents the maximum order of scattering events to archive the accuracy requirement. For each scattering order,

we have

$$\vec{\mathbf{I}}_{n+1}^{\uparrow}(\tau_i,\mu) = \vec{\mathbf{I}}_{n+1}^{\uparrow}(\tau_{i+1},\mu)\exp\{-(\tau_{i+1}-\tau_i)/\mu\} + \int_{\tau_i}^{\tau_{i+1}} \vec{\mathbf{J}}_n(t,\mu)\exp\{-(t-\tau_i)/\mu\}\,\mathrm{d}t/\mu, \tag{6a}$$

$$\vec{\mathbf{I}}_{n+1}^{\downarrow}(\tau_i,\mu) = \vec{\mathbf{I}}_{n+1}^{\downarrow}(\tau_{i-1},\mu)\exp\{-(\tau_i-\tau_{i-1})/\mu\} + \int_{\tau_{i-1}}^{\tau_i} \vec{\mathbf{J}}_n(t,\mu)\exp\{-(\tau_i-t)/\mu\}\,\mathrm{d}t/\mu \tag{6b}$$

with

$$\vec{\mathbf{J}}_n^{\uparrow\downarrow}(\tau,\mu) = \frac{\omega}{4}\int_{-1}^{1} \vec{\mathbf{M}}(\tau,\mu;\mu')\vec{\mathbf{I}}_n^{\uparrow\downarrow}(\tau,\mu')\,\mathrm{d}\mu' \tag{7}$$

and

$$\vec{\mathbf{J}}_0^{\uparrow\downarrow}(\tau,\mu) = \frac{\omega}{4\pi}\exp(-\tau/\mu_0)\vec{\mathbf{M}}(\tau,\mu;\mu_0)\mathbf{F} + \delta_{0m}(1-\omega)\mathbf{B}(T). \tag{8}$$

For the SOS method, the greatest challenge is the vertical integration of source term, $\mathbf{J}$, over optical depth. Suitable approximations would allow larger optical depth for each vertical homogeneous layer to speed up calculations. We approximate the source function by a linear-exponential function with optical depth in the domain $\tau_i < t < \tau_{i+1}$.

$$\vec{\mathbf{J}}(\tau,\mu) = (a+b\tau)\exp(-\beta\tau), \tag{9}$$

where a, b, and β can be solved analytically with $\vec{\mathbf{J}}(\tau_i,\mu)$, $\vec{\mathbf{J}}(\tau_{i+0.5},\mu)$ and $\vec{\mathbf{J}}(\tau_{i+1},\mu)$, and $\tau_{i+0.5} = (\tau_i+\tau_{i+1})/2$. The linear-exponential function approximation of source term has been proved to be accurate and efficient [23]. Given the above assumption, $\mathbf{I}_{n+1}$ can be integrated analytically and optical depth of each homogeneous layer can be relatively large. Therefore the computational time is saved substantially. We have also implemented a quadratic approximation of source function for integration over optical depth. Numerical simulations demonstrated that the linear–exponential approximation is more accurate than the quadratic approximation.

Furthermore, in order to calculate the Stokes vector at arbitrary angles and optical depths for a given vector solution at polar quadrature angles and vertical layers, we implement the angular interpolation method of post-processing source function (PPSF) in this VSOS code [24]. For solution at polar angle of μ^{out}, the source term for polar angle of μ^{out} can be written as

$$\vec{\mathbf{J}}_n^{\uparrow\downarrow}(\tau,\mu^{\mathrm{out}}) = \frac{\omega}{4}\int_{-1}^{1} \vec{\mathbf{M}}(\tau,\mu^{\mathrm{out}};\mu')\,\vec{\mathbf{I}}_n^{\uparrow\downarrow}(\tau,\mu')\,\mathrm{d}\mu'. \tag{10}$$

The source term of each successive order can then be integrated over optical depth as outline above (Eq. (6)). Therefore, the stokes vector at additional angles can be generated in a cost-effective way, and are more accurate than standard interpolation in the radiation intensity.

For the strong forward scattering media, the computational difficulties stem from the fact that strongly asymmetric phase function cannot be represented by polynomials of low order. As a result of increasing the number of streams for improving accuracy of calculation, the computational time will increase exponentially and the calculations based on the SOS method become exorbitant for

large optical depth cases. Taking advantage of the fact that the higher-order Legendre polynomial expansion terms contribute primarily to forward peak, the delta-m method truncates the Legendre polynomial to effectively remove the forward peak and has been proved to be a most reliable means in flux computations [25]. We implemented the delta-m transformation in our code to improve the computation efficiency and accuracy and suppress the false oscillation [25,26]. For the full vector radiative transfer algorithm (see Appendix A),

$$\begin{aligned}
&\alpha_{il}^{*} = (\alpha_{il} - f)/(1 - f),\\
&\beta_{il}^{*} = \beta_{il}/(1 - f),\\
&\tau^{*} = (1 - f\omega)\tau,\\
&\omega^{*} = (1 - f)\omega/(1 - f\omega).
\end{aligned} \tag{11}$$

After delta-m transformation from $\alpha, \beta, \omega, \tau$ to $\alpha^{*}, \beta^{*}, \omega^{*}, \tau^{*}$, the radiative transfer equation is the same as the original one with reduced forward scatterings.

2.2. Fourier decomposition of the phase matrix

Siewert [20] developed an efficient method for the Fourier components of the phase matrix, such that the components in a Fourier decomposition of the phase matrix could be expressed analytically in the basis of generalized spherical functions. The numerical implementation simply relies on a few recursive relations for the generalized spherical function. This method has been successfully implemented into various vector radiative transfer codes [16,18]. The accuracy and efficient of this expansion method has been tested in detail by De Haan et al. [16]. We adopted this method in the VSOS algorithm, and briefly sketch it here. For both $\vec{\mathbf{M}}_m^{\mathrm{c}}$ and $\vec{\mathbf{M}}_m^{\mathrm{s}}$ can be written as

$$\mathbf{M}_m^{\mathrm{c}}(\mu, \mu') = \mathbf{A}^m(\mu, \mu') + \mathbf{D}\mathbf{A}^m(\mu, \mu')\mathbf{D}, \tag{12a}$$

$$\mathbf{M}_m^{\mathrm{s}}(\mu, \mu') = \mathbf{A}^m(\mu, \mu')\mathbf{D} - \mathbf{D}\mathbf{A}^m(\mu, \mu') \tag{12b}$$

with

$$\mathbf{A}^m(\mu, \mu') = \sum_{\ell=m}^{L} (2\ell + 1)\mathbf{P}_\ell^m(\mu)\mathbf{B}_\ell\mathbf{P}_\ell^m(\mu'), \tag{13}$$

$$\mathbf{D} = \mathbf{diag}\{\mathbf{1}, \mathbf{1}, -\mathbf{1}, -\mathbf{1}\}, \tag{14}$$

$$\mathbf{P}_\ell^m(\mu) = \begin{bmatrix} \tilde{P}_\ell^m(\mu) & 0 & 0 & 0 \\ 0 & \tilde{R}_\ell^m(\mu) & -\tilde{T}_\ell^m(\mu) & 0 \\ 0 & -\tilde{T}_\ell^m(\mu) & \tilde{R}_\ell^m(\mu) & 0 \\ 0 & 0 & 0 & \tilde{P}_\ell^m(\mu) \end{bmatrix}, \tag{15}$$

$$\mathbf{B}_\ell = \begin{bmatrix} \alpha_1 & \beta_1 & 0 & 0 \\ \beta_1 & \alpha_2 & 0 & 0 \\ 0 & 0 & \alpha_3 & \beta_2 \\ 0 & 0 & -\beta_2 & \alpha_4 \end{bmatrix}, \tag{16}$$

where $\tilde{P}^m_\ell(\mu)$, $\tilde{R}^m_\ell(\mu)$ and $\tilde{T}^m_\ell(\mu)$ are normalized functions of $P^m_\ell(\mu)$, $R^m_\ell(\mu)$ and $T^m_\ell(\mu)$, respectively, by $\sqrt{(\ell-m)!/(\ell+m)!}$. $P^m_\ell(\mu)$ is the associate Legendre polynomial, $R^m_\ell(\mu)$ and $T^m_\ell(\mu)$ are generalized spherical functions, and given by

$$R^m_\ell = -\tfrac{1}{2}(i)^m[P^\ell_{m,2}(\mu) + P^\ell_{m,-2}(\mu)], \tag{17}$$

$$T^m_\ell = -\tfrac{1}{2}(i)^m[P^\ell_{m,2}(\mu) - P^\ell_{m,-2}(\mu)], \tag{18}$$

where $P^\ell_{m,n}(\mu)$ is the generalized spherical function

$$P^\ell_{m,n}(\mu) = \frac{(-1)^{\ell-m}(i)^{n-m}}{2^\ell(\ell-m)!}(1-\mu)^{-(n-m)/2}(1+\mu)^{-(n+m)/2}\frac{\mathrm{d}^{\ell-n}}{\mathrm{d}\mu^{\ell-n}}[(1-\mu)^{(\ell-m)}(1+\mu)^{(\ell+m)}]. \tag{19}$$

Furthermore, $\tilde{P}^m_\ell(\mu)$, $\tilde{R}^m_\ell(\mu)$ and $\tilde{T}^m_\ell(\mu)$ can be derived by recursion relations

$$\sqrt{[(\ell+1)^2-m^2]}\tilde{P}^m_{\ell+1} = (2\ell+1)\mu\tilde{P}^m_\ell - \sqrt{(\ell^2-m^2)}\tilde{P}^m_{\ell-1}, \tag{20a}$$

$$\frac{\sqrt{[(\ell+1)^2-m^2][(\ell+1)^2-4]}}{(\ell+1)}\tilde{R}^m_{\ell+1} = (2\ell+1)\left[\mu\tilde{R}^m_\ell - \frac{2m}{\ell(\ell+1)}\tilde{T}^m_\ell\right] - \frac{\sqrt{(\ell^2-m^2)(\ell^2-4)}}{\ell}\tilde{R}^m_{\ell-1}, \tag{20b}$$

$$\frac{\sqrt{[(\ell+1)^2-m^2][(\ell+1)^2-4]}}{(\ell+1)}\tilde{T}^m_{\ell+1} = (2\ell+1)\left[\mu\tilde{T}^m_\ell - \frac{2m}{\ell(\ell+1)}\tilde{R}^m_\ell\right] - \frac{\sqrt{(\ell^2-m^2)(\ell^2-4)}}{\ell}\tilde{T}^m_{\ell-1} \tag{20c}$$

with the initialization of

$$\tilde{P}^m_m(\mu) = \sqrt{\frac{(2m-1)!!}{(2m)!!}}(1-\mu^2)^{m/2}, \tag{21a}$$

$$\tilde{R}^m_m(\mu) = \sqrt{\frac{m(m-1)}{(m+1)(m+2)}}\frac{(1+\mu^2)}{(1-\mu^2)}\,\tilde{P}^m_m(\mu) \quad \text{for } m \geqslant 2,$$

$$\tilde{R}^1_1 = 0, \quad \tilde{R}^1_2 = -\frac{\mu}{2}\sqrt{(1-\mu^2)} \quad \text{for } m = 1,$$

$$\tilde{R}^0_0 = 0, \quad \tilde{R}^0_1 = 0 \quad \tilde{R}^0_2 = -\frac{\sqrt{6}}{4}(1-\mu^2) \quad \text{for } m = 0, \tag{21b}$$

$$\tilde{T}^m_m(\mu) = \sqrt{\frac{m(m-1)}{(m+1)(m+2)}}\frac{2\mu}{(1-\mu^2)}\,\tilde{P}^m_m(\mu) \quad \text{for } m \geqslant 2,$$

$$\tilde{T}^1_1 = 0, \quad \tilde{T}^1_2 = -\frac{1}{2}\sqrt{(1-\mu^2)} \quad \text{for } m = 1,$$

$$\tilde{T}^0_0 = 0, \quad \tilde{T}^0_1 = 0, \quad \tilde{T}^0_2 = 0 \quad \text{for } m = 0. \tag{21c}$$

The expansion coefficients in the matrix **B** are, then, determined by the following integrations:

$$\alpha^\ell_1 = \frac{1}{2}\int_{-1}^{1} a_1(\mu)P_\ell(\mu)\,\mathrm{d}\mu, \tag{22a}$$

$$\alpha^\ell_2 = \frac{1}{2}\int_{-1}^{1} [a_2(\mu)\tilde{R}^2_\ell(\mu) + a_3(\mu)\tilde{T}^2_\ell(\mu)]\,\mathrm{d}\mu, \tag{22b}$$

$$\alpha^\ell_3 = \frac{1}{2}\int_{-1}^{1} [a_3(\mu)\tilde{R}^2_\ell(\mu) + a_2(\mu)\tilde{T}^2_\ell(\mu)]\,\mathrm{d}\mu, \tag{22c}$$

$$\alpha^\ell_4 = \frac{1}{2}\int_{-1}^{1} a_4(\mu)P_\ell(\mu)\,\mathrm{d}\mu, \tag{22d}$$

$$\beta^\ell_1 = \frac{1}{2}\int_{-1}^{1} b_1(\mu)\tilde{P}^2_\ell(\mu)\,\mathrm{d}\mu, \tag{22e}$$

$$\beta^\ell_2 = \frac{1}{2}\int_{-1}^{1} b_2(\mu)\tilde{P}^2_\ell(\mu)\,\mathrm{d}\mu. \tag{22f}$$

As derived by Hovenier [27] and discussed by Siewert [20], there are two basic symmetry relations

$$\vec{\mathbf{M}}(\tau;\mu_i,\mu_j) = \mathbf{D}_1\vec{\mathbf{M}}(\tau;\mu_j,\mu_i)\mathbf{D}_1, \tag{23a}$$

$$\vec{\mathbf{M}}(\tau;-\mu_i,-\mu_j) = \mathbf{D}\vec{\mathbf{M}}(\tau;\mu_i,\mu_j)\mathbf{D}, \tag{23b}$$

where

$$\mathbf{D}_1 = \mathbf{diag}\{\mathbf{1}, \mathbf{1}, \mathbf{1}, -\mathbf{1}\}. \tag{24}$$

Based on above two basic symmetry relations, we can further derive the third useful symmetry relation that can simplify the implementation, and reduce the needs for calculating the elements of the phase matrix in another half.

$$\vec{\mathbf{M}}(\tau; \mu_i, -\mu_j) = \mathbf{D}_1\vec{\mathbf{M}}(\tau; -\mu_j, \mu_i)\mathbf{D}_1 = \mathbf{D}_1\mathbf{D}\vec{\mathbf{M}}(\tau; \mu_j, -\mu_i)\mathbf{D}\mathbf{D}_1 = \mathbf{D}_2\vec{\mathbf{M}}(\tau; \mu_j, -\mu_i)\mathbf{D}_2 \tag{25}$$

with

$$\mathbf{D}_2 = \mathbf{diag}\{\mathbf{1}, \mathbf{1}, -\mathbf{1}, \mathbf{1}\}. \tag{26}$$

3. Numeric tests and comparisons

To test our VSOS code, we computed Stokes components of I, Q, U, and V for several values of polar angle, azimuth angle and optical depth and compared with the benchmark results published in the literature [28]. We show one case of a homogeneous atmosphere of randomly orientated oblate spheroids with aspect ratio of 1.999987, size parameter of 3.0, and refractive index of $1.53 - 0.006i$. The single scattering albedo derived for this case is 0.975235 [29]. The total optical depth of the atmosphere is 1 with an underlying black surface. Our VSOS results are calculated using 32 streams in polar angle and 10 layers for the solar zenith angle of 50°. Fig. 1 shows stokes components of I, Q, and U, and degree of polarization as a function of polar angle at the top and at the bottom of the atmosphere. The solid and dashed lines represent results of the SOS model for downward radiation at the bottom of the atmosphere and upward radiation at the TOA, respectively; and the open circles represent the benchmark results. The agreement is excellent, and the accuracy is within 0.01%. Further extensive comparisons with the PolRadtran code developed by Evans and Stephens [15] are conducted for Mie scattering atmosphere (not shown here). The VSOS results agree well with the PolRadtran code.

The accuracy of the VSOS model depends on numbers of vertical layer and streams in angular quadrature, as well as orders of scattering. The smaller optical depth in each vertical layer and larger streams for angular quadrature will result in the higher accuracy, but at the expense of the computational speed. To speed up the calculation, we solve the successive scattering field based on discrete ordinate in angular coordinates and a linear-exponential approximation in optical depth. It is necessary to find the accuracy of integration over optical depth and interpolation in angle by conducting extensive numerical tests. We compute the benchmark stokes vector, represented as "true" in the following figures, with 32 streams and 0.01 optical depth for each layer. The total optical depth of the simulation slab is 1, the underlying surface is assumed to be black (albedo = 0). A Mie scattering phase function was used in the simulation. In the following discussion, we normalize the intensity, $\boldsymbol{I}$, by a fact of $\pi/\mu_0 F_0$, and define the polarization, $\boldsymbol{P}$, as $\sqrt{Q^2 + U^2}/I$.

First we test the linear–exponential approximation for different optical depths of a homogeneous layer to figure out the optimal optical depth for vertical integration. Fig. 2 shows differences of radiance and degree of polarization reaching at the TOA and at the surface for four different optical depths of vertical homogeneous layer. Since the difference of degree of polarization is very small, we

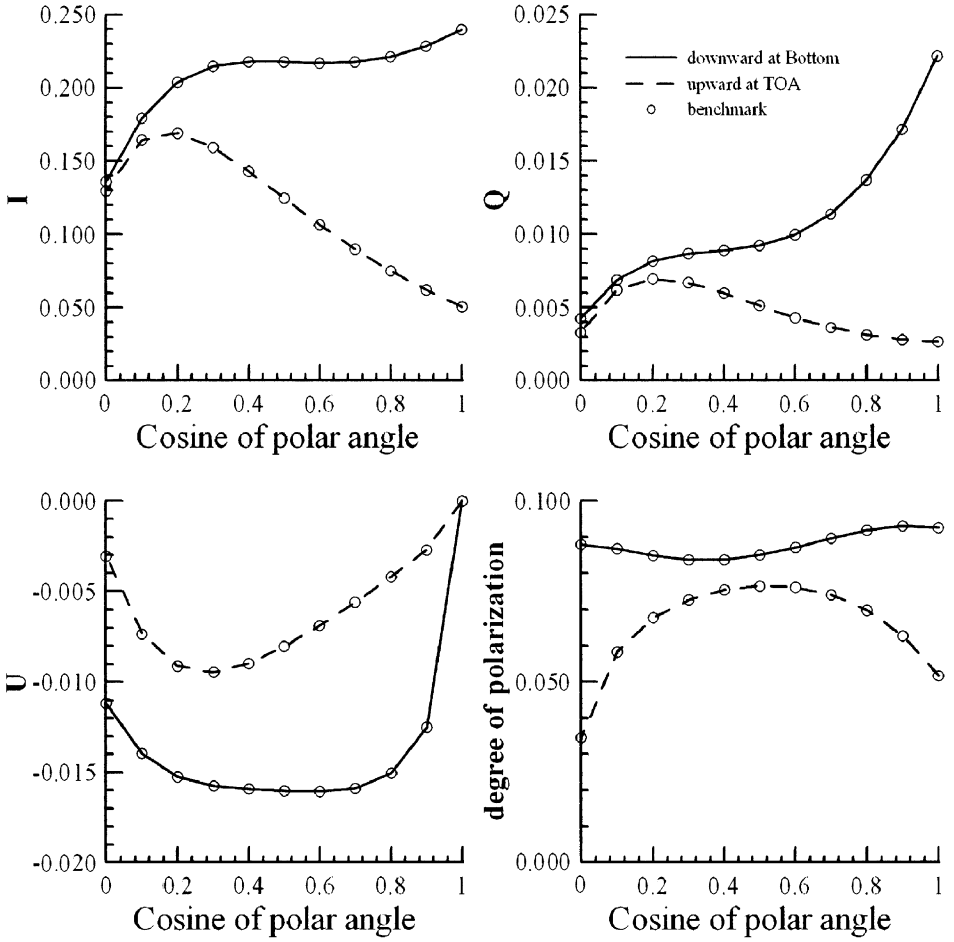

Fig. 1. Stokes parameters of I, Q, and U, and degree of polarization at the TOA (solid line) and at the bottom of the atmosphere (dashed line), open circles are benchmark.

multiply it by 100 as shown in the figures. In Fig. 2, the negative and positive cosine polar angles represent upward radiation at the TOA and downward radiation at the surface. As we expected, the accuracy of solution increases with increasing numbers of layer or decreasing optical depth of homogeneous layer for all sets of single scattering albedo. Differences of both radiance and degree of polarization decrease with decreasing of single scattering albedo in the atmosphere for a given optical depth of vertical homogeneous layer, since an increasing portion of photons that are absorbed in the atmosphere and do not participate in higher order scattering evens. For the worst scenario case with conservative scattering ($\varpi = 1$), shown in the top panels of Fig. 2, the maximum differences of radiance are 0.050%, 0.226%, 0.760%, and 2.238% for layer optical depths of 0.05, 0.1, 0.2, and 0.5, respectively. The maximum differences in degree of polarization are 0.00005, 0.00023, 0.00079, and 0.00266 for layer optical depths of 0.05, 0.1, 0.2, and 0.5, respectively. Based on current limitations of instrument capability, we set criteria of solution accuracy for radiance and degree of polarization

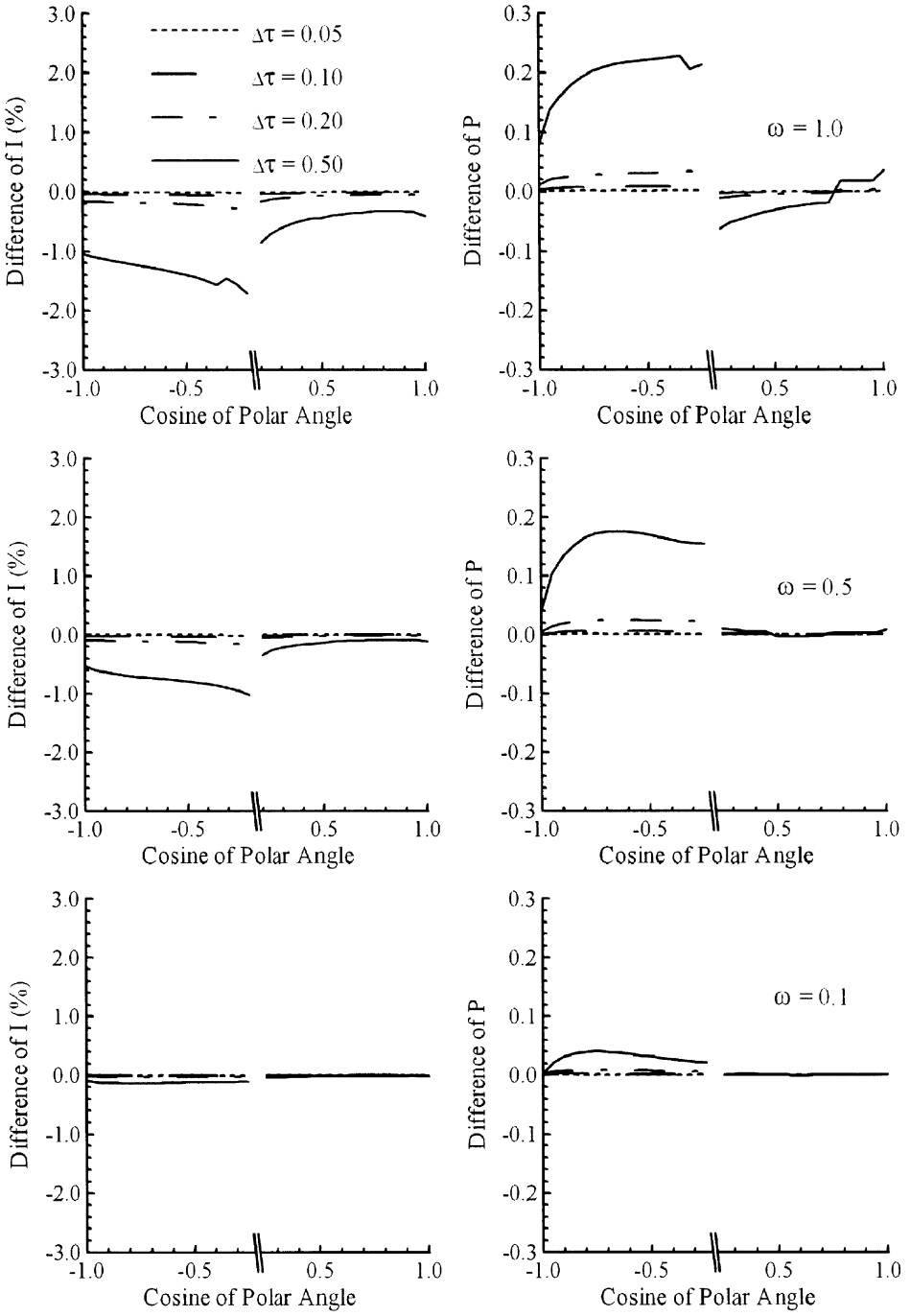

Fig. 2. Difference of upward radiance and degree of polarization at top of atmosphere and downward radiance and degree of polarization at surface.

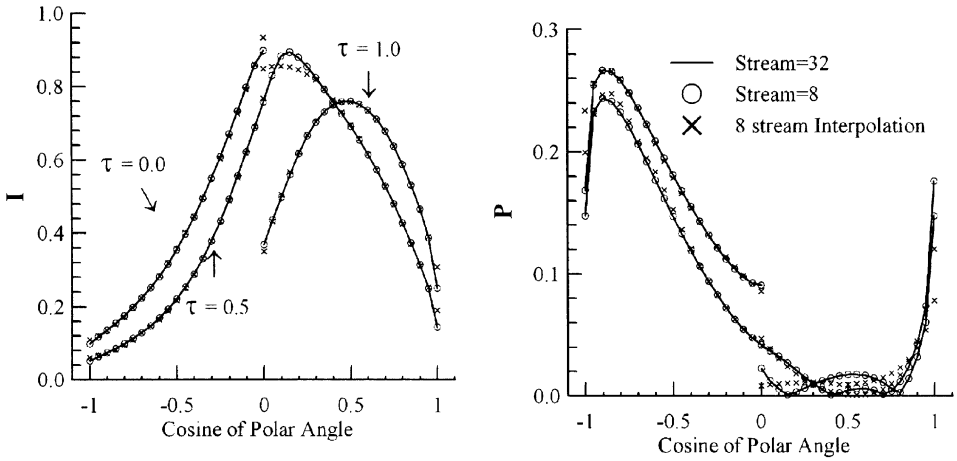

Fig. 3. Computed radiances and degrees of polarization at different optical depths with two interpolation methods.

as 1% and 0.1%, respectively. Therefore, optical depth of 0.2 is the optimal value for the VSOS integration over a homogeneous layer based on the linear–exponential approximation.

We further compare the PPSF analytic approach against a straightforward quadratic method for interpolating the angular distribution in the VSOS model. Fig. 3 shows computed radiances and degrees of polarization based on the PPSF approach and quadratic interpolations as a function of polar angle at the TOA and at the bottom of the atmosphere. Radiance and degree of polarization computed with 8-steam based on the PPSF approach agree well the benchmark (32-stream). The difference is less than 1%, which cannot be distinguished in the figure. The calculation for 8-stream takes, however, about a tenth of computational time for 32-stream. The superior agreement between 8-stream and 32-stream calculations of the VSOS model is due to: (1) the first-order scattering contributions of both cases are exact solutions without any interpolating, since J_0 is the same for both cases as the contribution of the direct beam of the sun; (2) the first-order scattering contributes significant portion of radiances and of degree of polarization (more discussion below); (3) the asymmetry factor is small: $g = 0.54$, therefore the difference between base solutions for both cases are relatively small (less than 0.2%). It demonstrates the advantage of the VSOS model on dealing with angular interpolation, such as simulating nadir or zenith observations. On the other hand, results based on quadratic interpolation show significant errors, particularly for cosine polar angles near ± 1. The results are consistent with the finding of Schultz and Stamnes [24].

The delta-m method transformation effectively removes the forward scattering, improving the computation efficiency. Fig. 4 show the comparison of Stokes parameters of I, Q, and U, and degree of polarization for delta-m transformation with 8, 12 and 16 streams. The atmospheric conditions are the same as previous case. The maximum differences of radiance between benchmark (64 streams without delta-m) and 8, 12, and 16 streams with delta-m are 8.25%, 1.649%, and 0.29%, respectively. The differences of polarization are even smaller, 3.127%, 0.238%, and 0.054% for 8, 12, and 16 streams with delta-m, respectively. As we expected, the upward fluxes at the TOA agree well: 0.71123, 0.71166, 0.71163, and 0.71161 for 8, 12, and 16 streams with delta-m and 64 streams without delta-m, respectively.

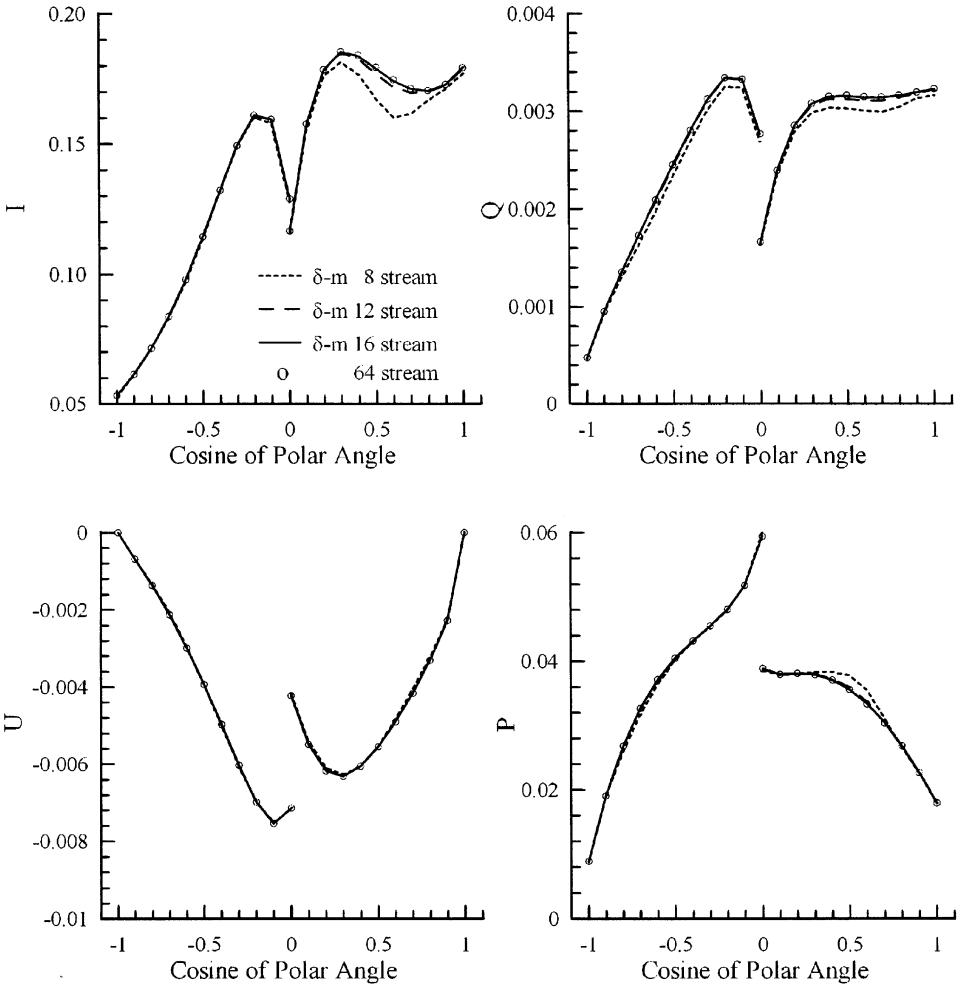

Fig. 4. Comparisons of Stokes parameters of I, Q, and U, and degree of polarization for delta-m of 8, 12 and 16 streams.

The most important issue for the SOS method is the convergence of the successive orders of scattering. Furthermore, the contribution of difference scattering orders will provide insight into the mechanisms of the scattering–absorption process. To reveal the consequence of scattering–absorption in the atmosphere and convergence of the VSOS model, we compute both radiance and degree of polarization for upward radiance at the TOA and downward radiance at the surface for conservative, modest and strong absorbed media with single scattering albedos of 1, 0.5 and 0.1, respectively. The optical properties are the same as in previous test cases. Fig. 5 shows cumulative contributions from various scattering orders. For conservative scattering condition, $\varpi = 1$, both radiance and degree of polarization converge when the order of scattering reaches about 10. However, for absorbed cases the convergence can be reached in 5 and 3 scattering orders for single scattering albedos of 0.5 and 0.1, respectively. Contributions of the first scattering to the total radiance are about 28%, 50%, and

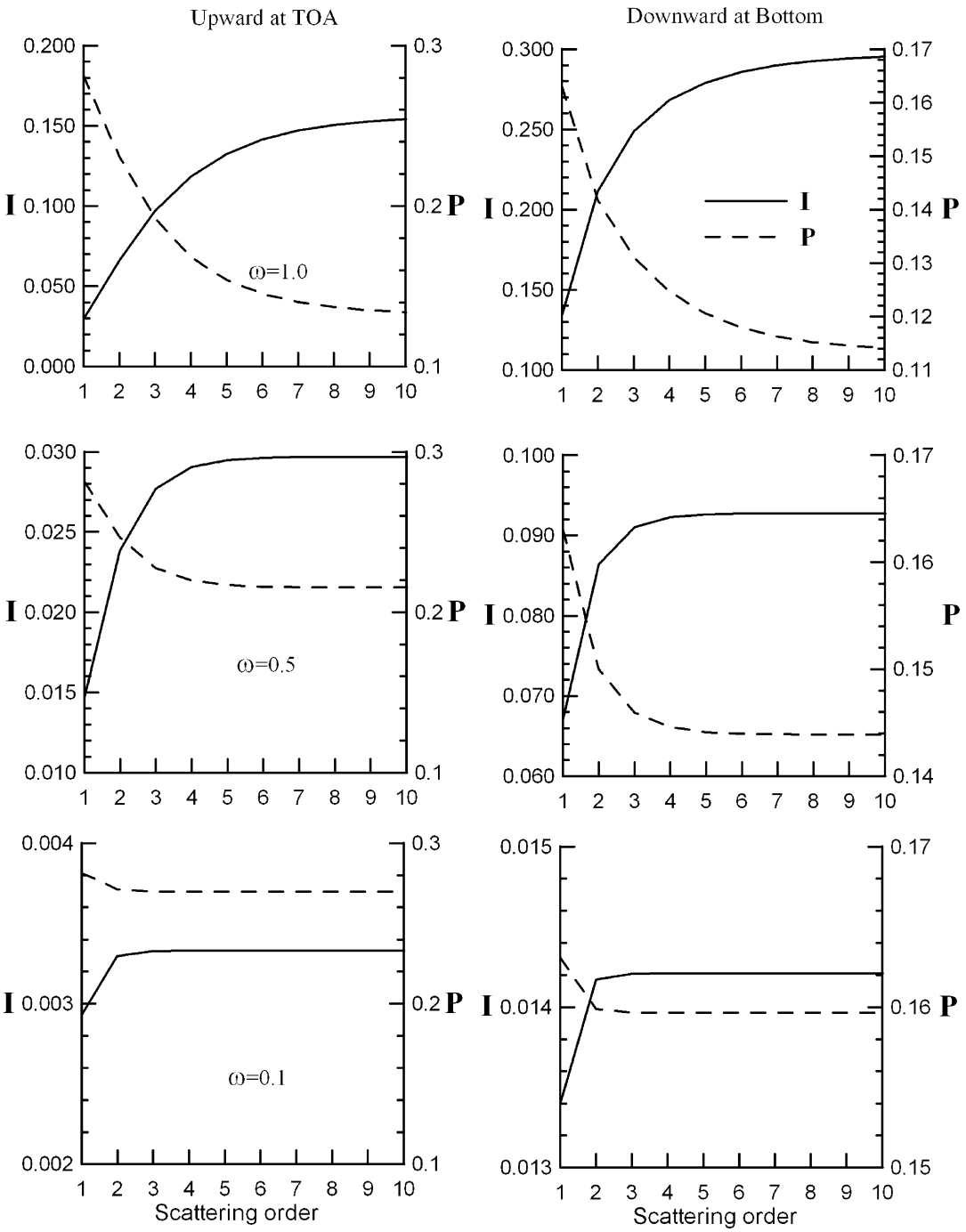

Fig. 5. Cumulative contributions from various scattering orders for three single scattering albedos of 1, 0.5, and 0.1. Solid line represents I and corresponds to the left axis and dashed line represents P and corresponds to the right axis.

95% of total radiance for single scattering albedos of 1, 0.5 and 0.1, respectively. It illustrates that we only need to accurately calculate the first one or two scattering orders with a simplified approach to deal with higher orders of scattering to speed up calculation for absorbing atmosphere.

4. Summary

Numerous instruments with polarization capability have been deployed on various platforms in retrieving atmospheric aerosol properties, determining size and shape of scattering particles, and discriminating surface and atmospheric contributions [5–11]. Almost all retrieval algorithms depend on a full calculation of radiation transfer in one way or another. To fully exploit the potentials of polarimetric measurements requires an accurate and fast vector radiative transfer model to interpret observations and for retrievals of atmospheric properties. Taking advantage of straightforward physics of the SOS method, we have developed a full vector radiative transfer model for vertically inhomogeneous plane–parallel media. To overcome issues of computational burden of convergence of the SOS method, we solved the successive scattering field based on discrete angular ordinates and a linear–exponential approximation in optical depth. We implemented a fast and accurately analytical expansion of Fourier decomposition, and used an analytic angular interpolation method of post-processing source function to accurately interpolate the Stokes vector at arbitrary angles for a given solution. It has been tested against the benchmarks for the case of randomly orientated oblate spheroids, illustrating a good agreement for each Stokes vector (0.01%). Sensitivity tests have been conducted to illustrate the accuracy of vertical integration and angle interpolation approaches. The optimal optical depth of homogeneous layer of about 0.2 for vertical integration will satisfy the need of accuracy of vector radiative transfer for current instrumental capability. Since the VSOS model explicitly separates the contribution of each scattering order, it has demonstrated the advantage on dealing with angular interpolation, such as simulating nadir or zenith observations using a few number of streams. Since the SOS method traces the photons for each scattering event, the inhomogeneous structure of the medium as well as gaseous absorption process can be incorporated in the calculation in terms of integration along the photon path. Further, it is very helpful for parameterization of radiative transfer for fast computation in remote sensing and global climate modeling. Sensitivity study also show that contributions of the first scattering to the total radiance are about 28%, 50%, and 95% of total radiance for single scattering albedos of 1, 0.5 and 0.1, respectively. It illustrates that we only need to accurately calculate the first one or two scattering orders with a simplified approach to deal with higher orders of scattering to speed up calculation for absorbing atmosphere, particularly for simulating gaseous absorption bands such as oxygen A-band and water vapor bands.

Acknowledgements

The authors thank Dr. L.C. Harrison for his valuable comments. This research was supported by the Office of Science (BER), U.S. Department of Energy, Grants DE-FG02-03ER6353, and by NASA JPL Contract 1207919.

Appendix A. δ-M transformation

Vector radiative transfer equation can be written as

$$\mu \frac{\mathrm{d}\vec{\mathbf{I}}(\tau,\mu,\phi)}{\mathrm{d}\tau} = -\vec{\mathbf{I}}(\tau,\mu,\phi) + \frac{\omega}{4\pi}\int_0^{2\pi}\int_{-1}^{1} \vec{\mathbf{M}}(\tau,\mu,\phi;\mu',\phi')\vec{\mathbf{I}}(\tau,\mu',\phi')\,\mathrm{d}\mu'\,\mathrm{d}\phi', \tag{A.1}$$

where

$$\vec{\mathbf{M}} = \vec{L}(\pi - i_2)\vec{\mathbf{P}}(\Theta)\vec{L}(-i_1), \tag{A.2}$$

where $\vec{\mathbf{P}}$ is the single scattering matrix

$$\vec{\mathbf{P}}(\Theta) = \begin{bmatrix} a_1 & b_1 & 0 & 0 \\ b_1 & a_2 & 0 & 0 \\ 0 & 0 & a_3 & b_2 \\ 0 & 0 & -b_2 & a_4 \end{bmatrix}. \tag{A.3}$$

L is the rotation matrix defined as (Liou, 1980)

$$\vec{L}(\chi) = \begin{bmatrix} 1 & 0 & 0 & 0 \\ 0 & \cos 2\chi & \sin 2\chi & 0 \\ 0 & -\sin 2\chi & \cos 2\chi & 0 \\ 0 & 0 & 0 & 1 \end{bmatrix}. \tag{A.4}$$

Based on delta-m transformation, the scattering matrix can be replaced by the summation of a delta function for the forward peak and a smoothed function,

$$\vec{\mathbf{P}}(\tau,\mu,\mu') = 2f\delta(1-\cos(\Theta))\vec{\mathbf{E}} + (1-f)\vec{\mathbf{P}}^{*}, \tag{A.5}$$

where $f = \alpha_{1,2M}$; $\vec{\mathbf{E}} = \mathbf{diag}\{1,1,1,1\}$, $\vec{\mathbf{P}}^{*}$ has the same form of Eq. (A.3). Substituting Eq. (A.5) into Eq. (A.1), we have

$$\mu \frac{\mathrm{d}\vec{\mathbf{I}}(\tau,\mu,\varphi)}{\mathrm{d}\tau} = -(1-f\omega)\vec{\mathbf{I}}(\tau,\mu,\varphi) + (1-f)\frac{\omega}{4\pi}\int_0^{2\pi}\int_{-1}^{1} \vec{\mathbf{M}}^{*}(\tau,\mu,\varphi;\mu',\varphi')\vec{\mathbf{I}}(\tau,\mu',\varphi')\,\mathrm{d}\mu'\,\mathrm{d}\varphi', \tag{A.6}$$

where

$$\vec{\mathbf{M}}^{*} = \vec{L}(\pi - i_2)\vec{\mathbf{P}}^{*}(\Theta)\vec{L}(-i_1). \tag{A.7}$$

If we define

$$\tau^{*} = (1-f\omega)\tau,$$
$$\omega^{*} = (1-f)\omega/(1-f\omega). \tag{A.8}$$

Eq. (A.8) has been transformed to

$$\mu \frac{\mathrm{d}\vec{\mathbf{I}}(\tau^*,\mu,\varphi)}{\mathrm{d}\tau^*} = -\vec{\mathbf{I}}(\tau^*,\mu,\varphi) + \frac{\omega^*}{4\pi}\int_0^{2\pi}\int_{-1}^{1}\vec{\mathbf{M}}^*(\tau^*,\mu,\varphi;\mu',\varphi')\vec{\mathbf{I}}(\tau^*,\mu',\varphi')\,\mathrm{d}\mu'\,\mathrm{d}\varphi'. \tag{A.9}$$

Eq. (A.9) has the same form as Eq. (A.1). In Eqs. (A.1) and (A.9), the coefficients of a_i, b_i, a_i^*, b_i^* and δ function can be expanded as spherical polynomials

$$a_i = \sum_{\ell=0}^{2M-1}(2\ell+1)\alpha_{i\ell}\xi_{il}, \quad i=1,2,3,4,$$

$$b_i = \sum_{\ell=0}^{2M-1}(2\ell+1)\beta_{i\ell}\tilde{P}_\ell^2, \quad i=1,2, \tag{A.10}$$

$$a_i^* = \sum_{\ell=0}^{2M-1}(2\ell+1)\alpha_{i\ell}^*\xi_{i\ell}, \quad i=1,2,3,4,$$

$$b_i^* = \sum_{\ell=0}^{2M-1}(2\ell+1)\beta_{i\ell}^*\tilde{P}_\ell^2, \quad i=1,2, \tag{A.11}$$

$$\delta(1-\cos(\Theta))\vec{\mathbf{E}} = \frac{1}{2}\sum_{\ell=0}^{2M-1}(2\ell+1)\,\mathbf{diag}\{\xi_{1\ell},\xi_{2\ell},\xi_{3\ell},\xi_{4\ell}\}, \tag{A.12}$$

where $\xi_{i\ell}$ is $P_\ell, (\tilde{R}_\ell^2+\tilde{T}_\ell^2), (\tilde{R}_\ell^2+\tilde{T}_\ell^2)$ and P_ℓ for $i=1,2,3$, and 4, respectively. Substituting above three equations into Eq. (A.5), the expanded coefficients after transformation can be given as

$$\alpha_{i\ell}^* = (\alpha_{i\ell}-f)/(1-f), \quad i=1,2,3,4,$$

$$\beta_{i\ell}^* = \beta_{i\ell}/(1-f), \quad i=1,2. \tag{A.13}$$

References

[1] Genevieve R, Herman M. Polarization of light reflected by crop canopies. Remote Sensing Environ 1991;38:63–75.

[2] Breon FM, Tanre D, Lecomte P, Herman M. Polarized reflectance of bare soils and vegetation: measurements and models. IEEE Trans Geosci Remote Sensing 1995;33(2):487–99.

[3] Mishchenko MI, Travis LD. Satellite retrieval of aerosol properties over the ocean using polarization as well as intensity of reflected sunlight. J Geophys Res 1997a;102(D14):16989–7013.

[4] Mishchenko MI, Travis LD. Satellite retrieval of aerosol properties over the ocean using measurements of reflected sunlight: effect of instrumental errors and aerosol absorption. J Geophys Res 1997b;102(D12):13543–53.

[5] Deuze JL, Goloub P, Herman M, Marchand A, Perry G, Susana S, Tanre D. Estimate of the aerosol properties over the ocean with POLDER. J Geophys Res 2000;105(D12):15329–46.

[6] Deuze JL, Breon FM, Devaux C, Goloub P, Herman M, Lafrance B, Maignan F, Marchand A, Nadal F, Perry G, Tanre D. Remote sensing of aerosols over land surfaces from POLDER-ADEOS-1 polarized measurements. J Geophys Res 2001;106(D5):4913–26.

[7] Boucher O, Tanre D. Estimation of the aerosol perturbation to the Earth's radiative budget over oceans using POLDER satellite aerosol retrievals. Geophys Res Lett 2000;27(8):1103–6.

[8] Riedi J, Doutriaux-Boucher M, Goloub P, Couvert P. Global distribution of cloud top phase from POLDER/ADEOS I. Geophys Res Lett 2000;27(12):1707–10.

[9] Parol Frederic, Descloitres Jacques, Fouquart Yves. Cloud optical thickness and albedo retrievals from bidirectional reflectance measurements of POLDER instruments during ACE-2. Tellus (B): Chem Phys Meteorol 2000;52B(2): 888–908.
[10] Breon Francois-Marie, Colzy Stephane. Global distribution of cloud droplet effective radius from POLDER polarization measurements. Geophys Res Lett 2000;27(24):4065–8.
[11] Vanbauce C, Buriez JC, Parol F, Bonnel B, Seze G, Couvert P. Apparent pressure derived from ADEOS-POLDER observations in the oxygen A-band over ocean. Geophys Res Lett 1998;25(16):3159–62.
[12] Mishchenko MI. Multiple scattering of polarized light in anisotropic plane-parallel media. Trans Theory Stat Phys 1990a;19:293–316.
[13] Mishchenko MI. Extinction and polarization of transmitted light by partially aligned nonspherical grains. Astro J 1990b;367:561–74.
[14] Mishchenko MI. The fast invariant imbedding method for polarized light: computational aspects and numerical results for Rayleigh scattering. JQSRT 1990c;43:163–71.
[15] Evans KF, Stephens GL. A new polarized atmospheric radiative transfer model. JQSRT 1991;46(5):413–23.
[16] De Haan JF, Bosma PB, Hovenier JW. The adding method for multiple scattering computations of polarized light. Astron Astrophys 1987;183:371–91. and reference herein.
[17] Weng F. A multi-layer discrete-ordinate method for vector radiative transfer in a vertically-inhomogeneous, emitting and scattering atmosphere–I. theory. J Quant Spectrosc Radiat Transfer 1992;47:19–33.
[18] Schulz FM, Stamnes K, Weng F. VDISORT: an improved and generalized discrete ordinate method for polarized (vector) radiative transfer. J Quant Spectrosc Radiat Transfer 1999;61:105–122.
[19] Liou KN, Rao NX. Radiative transfer in cirrus clouds. Part IV. On cloud geometry, inhomogeneity, and absorption. J Atmos Sci 1996;53:3046–65.
[20] Siewert CE. On the phase matrix basic to the scattering of polarized light. Astron Astrophys 1982;109:195–200.
[21] Chandrasekhar S. Radiative transfer. Oxford: Oxford University Press; 1950. (republished by Dover Publication; 1960).
[22] van de Hulst HC. Light scattering by small particles. New York: Wiley; 1957.
[23] Kylling A, Stamnes K. Efficient yet accurate solution of the linear transport equation in the presence of internal sources: the exponential-linear-in depth approximation. J Comput Phys 1992;102:265–276.
[24] Schulz FM, Stamnes K. Angular distribution of the Stokes vector in a plane-parallel, vertically inhomogeneous medium in the vector discreteordinate radiative transfer (VDISORT) model. JQSRT 2000;65:609–20.
[25] Wiscombe WJ. Delta-*m* method: rapid yet accurate radiative flux calculations for strongly asymmetric phase functions. J Atmos Sci 1977;34(9):1408–22.
[26] Duan M. Simultaneously retrieval of atmospheric aerosol optical thickness and surface albedo over land by using polarized radiance as well as scalar radiance from POLDER measurement. PhD dissertation, Institute of Atmospheric Physics, Chinese Academy of Sciences, 2001.
[27] Hovenier JW. Symmetry relationships for scattering of polarized light in a slab of randomly oriented particles. J Atmos Sci 1969;26:488–99.
[28] Wauben WMF, Hovenier JW. Polarized radiation of an atmosphere containing randomly-oriented spheroids. JQSRT 1992;47(6):491–504.
[29] Kuik F, De Haan JF, Hovenier JW. Benchmark results for single scattering by spheroids. JQSRT 1992;47(6): 477–89.